Article

Performance Estimation: CCL WPT Topologies with Helical Coils

Chien-Lung Chen [1] and Chung-Wen Hung [2,*]

1   Doctorial Program, Graduate School of Engineering Science and Technology, 123 University Road, Section 3, Douliu 64002, Taiwan; d10310008@yuntech.edu.tw
2   Department of Electrical Engineering, National Yunlin University of Science and Technology, 123 University Road, Section 3, Douliu 64002, Taiwan
*   Correspondence: wenhung@yuntech.edu.tw; Tel.: +886-5-534-2601 (ext. 4265)

Abstract: The radius of the coil, the number of turns of the windings, and the parasitic resistances of energy-storing elements affect the performances of wireless power transfer systems. We aimed to study the effects of coil parameters on a wireless power transfer system with the capacitor–capacitor–coupling coil (CCL)-based circuit using numerical simulations. The power transfer system topologies, including series–CCL (S–CCL), CCL–S, and CCL–CCL, were studied vis-à-vis coil parameters. The helical coil and the system topologies were modeled using MATLAB, and the performances of the topologies were examined in comparison to the series–series (S–S) topology. The variables used in the simulations included the radius and number of turns, the parasitic resistance that was merged in the impedance, and the reactance of energy-storing elements. Subsequently, the performances of the topologies were estimated by numerical simulations under several circumstances. The simulation results showed that the parasitic resistance of the coupling coil affects the performances of the topologies directly. The coupling coils with smaller geometries are beneficial to power transfer in the wireless power transfer system and may further contribute to miniaturization.

Keywords: CCL circuit; helical coil; parasitic resistance; topology; wireless power transfer

1. Introduction

Wireless power transfer (WPT) has received immense interest as it can be used in applications where power transfer must be performed without the use of wires. Various composite and hybrid compensation topologies have been proposed for WPT. The composite series–parallel-combination resonant circuit (SPRC) has been proposed for magnetic resonant wireless power transfer (MR-WPT), which offers enhanced performance compared to classical topologies [1]. Hybrid topologies, which comprise the variants of composite SPRCs, have also been proposed. A capacitor–capacitor–coupling coil (CCL)-based circuit is one of the hybrid topologies [2]; its structure is composed of a series capacitor connecting the power source and the coupling coil and a shunt capacitor connecting the coupling coil in parallel. The advantage of the CCL circuit is that its circuit quality factor (Q factor) can be adjusted by the ratio between the series and shunt capacitances; the current flowing through the coupling coil is twice that of the power source when both series and shunt capacitors are identical [3].

Kim et al. (2021) estimated the performances of WPT system topologies with CCL circuits [4] based on a fixed operating frequency and a specific parasitic resistance of energy-storing elements. The transmitting power and the power transfer efficiency of various CCL-based WPT system topologies were compared by changing the coupling air gap, while Imura et al. (2009) [5] showed that the magnitude of mutual inductance between two coupling coils changes with the coupling air gap. They calculated the mutual inductance using the Neumann formula, which involves the radius, the number of turns of the coupling coil, and the air gap. Therefore, the change in the air gap affects the mutual

inductance. Meanwhile, Imura et al. (2009) [6] proposed that different mutual inductances generate differences in the resonant frequencies of system topologies.

Moreover, the alternating-current (AC) resistance in the coupling coil (R_{ac}) and the equivalent series resistance (ESR) in the capacitor are influenced by frequency variations. In addition, coil parameters such as the type and geometry of the coupling coil and the material permeability around the coupling coil significantly impact the performance of WPT [7]. Therefore, the performances of CCL-based WPT system topologies must be revealed thoroughly considering these parameters.

Misalignment between coupling coils also affects the performances of WPT systems as the geometries of helical coils and the air gap.

As the CCL circuit has a high Q factor, the performance of the system topologies using the CCL circuit is worth studying. In this work, the performance of the system topologies was estimated by MATLAB simulation depending on the different geometric parameters of the coupling coil, the air gaps, and the misalignment between the coupling coils for providing further development in the wireless power transfer system.

According to the simulated results, the AC parasitic resistance in the coupling coil will increase with the number of turns added; there will be a significant effect on the CCL circuit by the increment of the AC parasitic resistance, thereby reducing the efficiency of the circuit and then declining the transmitting power and power transfer efficiency.

The CCL circuit placed on the transmitting and receiving sides is not necessarily to gain optimum performance in the system topology as the relationship of the parasitic resistance. Reducing the parasitic resistance in the system topology is a subject for further development in wireless power transfer.

2. Materials and Methods

WPT system equivalent topologies with CCL-based circuits are illustrated in Figure 1.
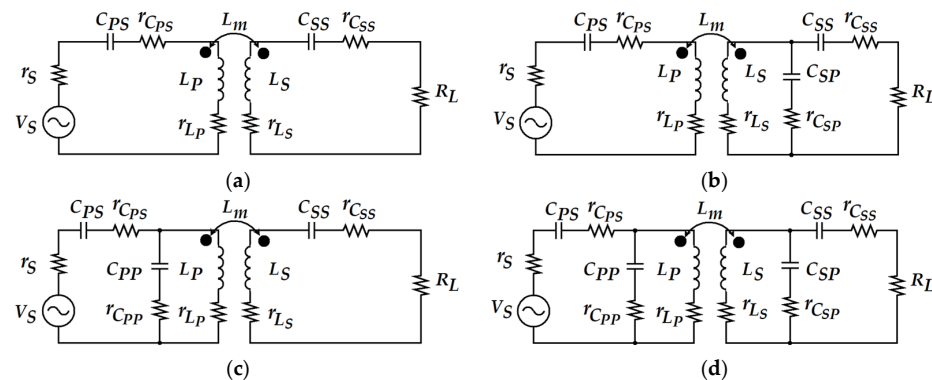
Figure 1. Equivalent topology of wireless power transfer system (**a**) S–S; (**b**) S–CCL; (**c**) CCL–S; (**d**) CCL–CCL.

The S–S, S–CCL, CCL–S, and CCL–CCL topologies were studied, whereas the S–S topology was also investigated for comparison. The S–CCL system topology in Figure 1b uses a series resonant circuit for the transmitter; the receiver employs the CCL-based circuit. Figure 1c shows the CCL–S system topology that employs the CCL resonant circuit for the transmitter and uses the series circuit for the receiver; the topology is the opposite of the previously mentioned S–CCL topology. The CCL–CCL system topology is shown in Figure 1d. Its structure is symmetrical; thus, the transmitter and receiver sides all employ identical CCL circuits.

Furthermore, each resistor has different implications; r_S represents the inner resistance of the power source; the parasitic resistances of all energy-storing elements are represented by r_{CX}; and r_{LX} represents the AC resistor of the coupling coils, respectively. R_L represents the equivalent resistance of the system load. The power source for topology is named V_S; it is likely a full-bridge or half-bridge, and even a class D or E inverts the drive circuit.

Kim et al. (2018) reported that the performance of a WPT system topology with a CCL-based circuit can be estimated from the transmitting power and the power transfer efficiency [8]. The transmitting power is the power absorbed by the system load, whereas the magnitude of the transmitting power, P_{out}, can be derived from the following equation:

$$P_{out} = \frac{4k^2Q_1Q_2}{\left(1+k^2Q_1Q_2\right)^2}\delta_T\delta_R P_{out,max} \tag{1}$$

The components in the above transmitting power equation mainly include the coupling coefficient, k, the circuit quality factor (Q factor), and the parasitic resistance in the topology. In the expression, δ_T and δ_R represent the circuit efficiencies of the transmitter and the receiver, respectively. The relation expression for efficiencies is shown in Equations (2) and (3).

$$\delta_T = \frac{r_S}{r_1+r_S} \tag{2}$$

$$\delta_R = \frac{r_L}{r_2+r_L} \tag{3}$$

here, r_1 and r_2 are the total parasitic resistances of the energy-storing elements on the transmitter and the receiver, respectively; that is, the sum of the ESR for the capacitor and Rac for the coupling coil. $P_{out,max}$ is the achievable transmitting power from the power source and is expressed as the following:

$$P_{out,max} = \frac{V_{IN}^2}{4r_s} \tag{4}$$

The power transfer efficiency is defined as follows:

$$\eta = \left[1 - \frac{r_1}{r_1+k^2Q_1Q_2(r_1+r_s)}\right]\delta_R \tag{5}$$

In the equation, the power transfer efficiency for the system topology is constructed by the parasitic resistance on the transmitter, r_1, the Q factor of both sides, Q_1 and Q_2, the coupling coefficient, k, as well as the efficiency of the receiver, δ_R.

The parasitic resistances, Q factor, and coupling coefficient are expressed in the definitions of the transmitting power and the power transfer efficiency. It could be inferred that these parameters determine the performance of the WPT system.

Meanwhile, the parasitic resistances in the energy-storing elements of the topologies vary depending on the operating frequencies.

The resistance increases with the operating frequency, as shown in Figure 2a,b. The corresponding parasitic resistances of the energy-storing elements increase with the operating frequency.

(a)

(b)
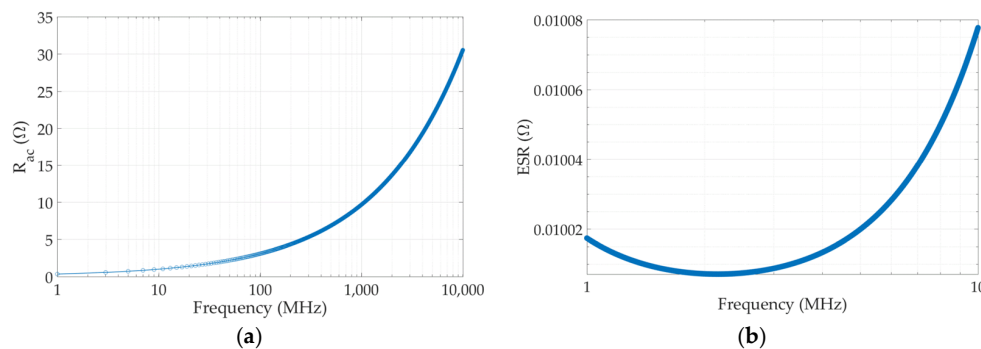
Figure 2. Variances at different frequencies for (**a**) AC resistance of the coupling coil and (**b**) equivalent series resistance, ESR, of the capacitor.

Imura (2020) [9] reported that the parasitic resistance in the coupling coil was produced by the winding wire that suffers the skin effect. The resistance of a helical coupling coil can be derived by the following formula:

$$R_{ac} = \frac{\rho l}{\pi \delta (D - \delta)},$$ (6)

where ρ presents the resistivity of the winding wire, and l is the total length of the winding wire. δ in the denominator presents the skin depth, and D is the diameter of the winding wire. The skin depth of the winding wire is defined as the following:

$$\delta = \sqrt{\frac{2}{\omega \sigma \mu}}$$ (7)

where, σ is the conductivity of the winding wire, and μ is the permeability of the winding wire. ω is the angular frequency of the current flowing through the winding wire.

Based on these equations, the skin effect decreases while the parasitic resistance increases with the increased current frequency, indicating that the parasitic resistance of the coupling coil increases at a higher operating frequency. This likely affects the driving current for the coupling coil and the quality factor of the circuit.

Lindquist (1978) reported that the ESR of the capacitor depends on the dissipation factor (DF) [10]. The relation between the ESR and DF is given as the following:

$$ESR = DF \times X_C$$ (8)

The ESR is the product of the DF and the reactance of the capacitor, X_C. The DF is the ratio of power loss to the reactive power of the capacitor equivalent circuit. The total impedance of the equivalent circuit for the capacitor is given as

$$Z_{C,eq} = R + j(X_L - X_C) = \text{Re}\, Z_{C,eq}(j\omega) + j\text{Im}\, Z_{C,eq}(j\omega),$$ (9)

and the dissipation factor, DF, for the capacitor is defined as

$$DF = \frac{\text{power loss}}{\text{reactive power in}} = \frac{R}{X}$$ (10)

The reactance and DF of the capacitor rely on the angular frequency. Therefore, the ESR of the capacitor versus the operating frequency renders a quadratic curve. Namely, there is a frequency at which the lowest ESR can be obtained for the capacitor.

The frequency point with the lowest DF value refers to the self-resonant frequency of the capacitor. The DF value decreases with the frequency in the frequency range lower than the self-resonant frequency. Meanwhile, if the operating frequency is higher than the self-resonant frequency of the capacitor, the DF value rises gradually.

The DF of the capacitor varies with the operating frequency caused by the equivalent inductive and capacitive reactance of the capacitor. As shown in (9), it presents the impedance in the capacitor with various operating frequencies. There will be the smallest value of the impedance when the capacitor operates at the self-resonant frequency, since the inductive and the capacitive reactance are equal. Meanwhile, the DF will also end up being being small, due to the impedance of the capacitor being the smallest. As discussed above, when the capacitor operating frequency becomes gradually less than the self-resonant frequency, the variation in the operating frequency causes the capacitive reactance to be greater than the inductive one, enlarging the impedance and then increasing the DF of the capacitor. Relatively, when the capacitor operating frequency increases gradually from the self-resonant one, equivalent inductive reactance becomes more than the capacitive one, rendering the impedance increase and enlarging the DF simultaneously.

Kim et al. (2017) showed that the Q factor for the circuit is the ratio of the energy in the energy-storing elements to the dissipation of the entire topology, multiplied by the angular frequency [11]. The relation equation for the Q factor is expressed as

$$Q = \omega \times \frac{E_{stored}}{P_{loss}} \tag{11}$$

According to Kim et al. (2021) [4], the circuit Q factor for the series resonant circuit can be derived by

$$Q_S = \omega \frac{L}{R + r_{t,S}} \tag{12}$$

and the Q factor of the CCL resonant circuit is

$$Q_{CCL} = \omega \frac{L}{R + r_{t,CCL}} \left(1 + \frac{1}{y}\right)^2 \tag{13}$$

In Equation (13), y is the ratio of the series capacitance, C_{XS}, to the shunt capacitance, C_{XP}. Here, X represents the side of the capacitor placement, P represents the capacitor placed on the transmitter side, and S represents the capacitor placed on the receiver, e.g., since a series capacitor is placed on the transmitter side, the symbol is marked as C_{PS}. R represents the resistance on the circuit; on the transmitter side, R represents the inner resistance of the power source, r_S; on the receiver side, R becomes the equivalent resistance of the load, R_L.

$r_{t,S}$ and $r_{t,CCL}$ are the total parasitic resistances in the series and CCL circuits, respectively. That can be derived by following Equations (14) and (15).

$$r_{t,S} = r_L + r_C \tag{14}$$

$$r_{t,CCL} = r_{C_{XS}} + \left(1 + \frac{1}{y}\right)^2 r_L + r_{C_{XP}} \tag{15}$$

In the Equations (14) and (15), r_L represents the resistance in AC for the helical coil; and r_C, $r_{C_{XS}}$, and $r_{C_{XP}}$ are the ESRs for the capacitors.

The coupling coefficient, k, displayed in the previous Equations (1) and (5) is the ratio of the linkage flux between the coupling coils [12]:

$$k = \frac{L_m}{\sqrt{L_1 L_2}} \tag{16}$$

The coupling coefficient depends on the mutual inductance between the coupling coils and the self-inductance of each coil. The range for the coupling coefficient is $0 \leq k \leq 1$.

For this work, the coupling coil for simulation uses the helical coil. The parameters of the helical coupling coil are displayed in Figure 3.

Figure 3a represents an illustration of a single helical coil; the geometry of the helical coil comprises the radius of the helical coil, a; the pitch between the conducting wires, p; the length of the coupling coil, l; and the width of the conducting wire, D. Furthermore, the air core is assumed in the helical coil; the air core is used to avoid differences in the permeabilities of the materials. Moreover, the permeability of the material varies noticeably with the environmental temperature. Figure 3b displays the air gap between two helical coupling coils, g. The coupling coils are placed coaxially without misalignment. In the case of misalignment, lateral and angled misalignments between two coupling coils were studied. The lateral misalignment is shown in Figure 3c; the central axials of two coupling coils are not coaxial and exist at a distance, c. Additionally, Figure 3d presents the misalignment in the degrees of α.
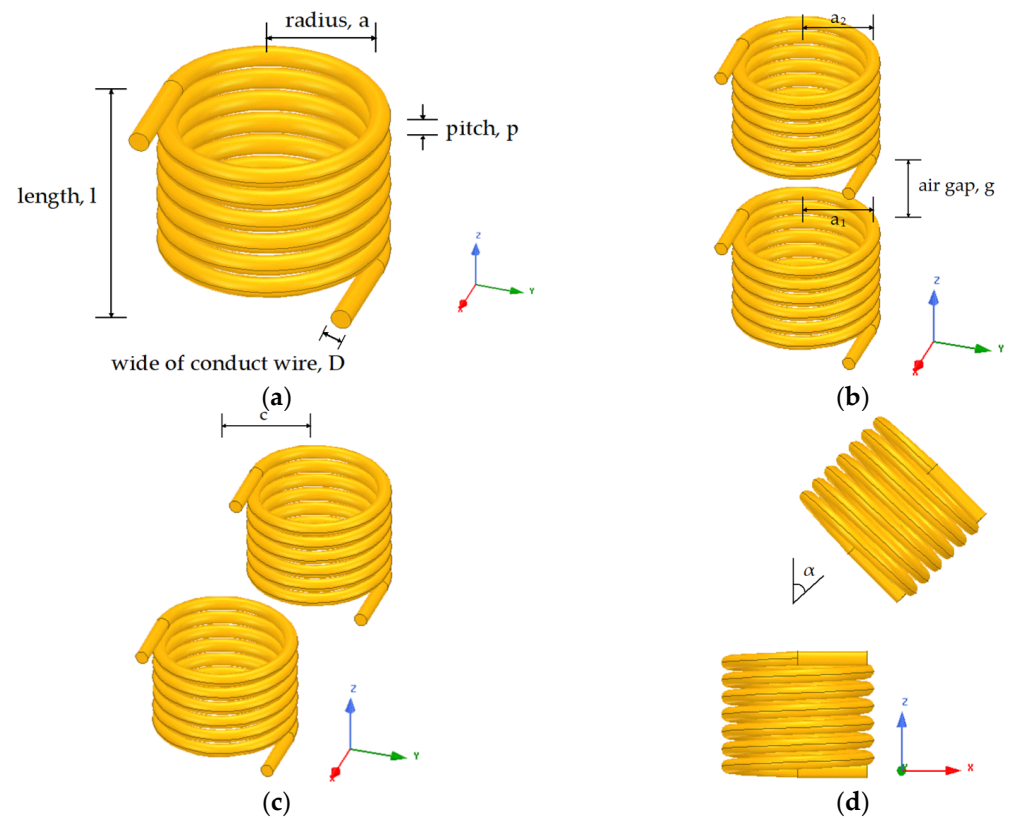
Figure 3. (**a**) Helical coupling coil and (**b**) air gap between two coupling coils; (**c**) lateral misalignment and (**d**) angled misalignment.

The angled misalignment refers to two coupling coils misaligned at an angle, α.

For the equation of the coupling coefficient, the self-inductance (Joost, 2015) [13] of the helical coupling coil according to Figure 3a is expressed as the following:

$$L = \frac{\mu \pi a^2 N^2}{l} K, \tag{17}$$

The self-inductance of the helical coil depends on its geometry, the permeability of the core material, μ, and the Nagaoka coefficient, K, for correction. The geometry of the coil refers to the radius of the helical coil, a; the number of turns, N; the length of the helical coil, l.

Mutual inductance is a property in which the primary coil affects the voltage and the current in the secondary coil, whereas the current relates to the geometry of the coupling coils. The equation, Neumann formula, of mutual inductance for the helical coupling coil without consideration of the misalignment between the coupling coils (Zhang, 2019) [14] is expressed as

$$L_m = \frac{\mu}{4\pi} \int_0^{2N_1\pi} \int_0^{2N_2\pi} \frac{a_1 a_2 \cos(\theta - \varphi) + (p/2\pi)^2}{\sqrt{a_1^2 + a_2^2 - 2a_1 a_2 \cos(\theta - \varphi) + [(p/2\pi)(\theta - \varphi) - g]^2}} d\theta d\varphi, \tag{18}$$

a_1 and a_2 represent the radii of the helical coils, and p represents the pitch between the winding wire of the helical coil. The air gap between the helical coil is symbolized as g, and $\cos(\theta - \varphi) + (p/2\pi)^2$ is the product of line elements. N_1 and N_2, marked at the upper bounds of the double integral, are the number of turns for the helical coupling coils, and μ is the permeability of the material inserted into the coupling coils.

Considering there is a misalignment between two helical coupling coils, the equation of mutual inductance needs to consider the lateral distance or the angle according to the

Cartesian coordinate system. The mutual inductance considering the misalignment is described as

$$L_m = \frac{\mu}{4\pi} \int_0^{2N_1\pi} \int_0^{2N_2\pi} \frac{g(\alpha, c)}{y(\alpha, c)} d\theta d\varphi, \tag{19}$$

The function $g(\alpha, c)$ given in the numerator in the double integral is described as

$$a_1 a_2 \sin\theta \sin\varphi + a_1 a_2 \cos\alpha \cos\theta \cos\varphi + \left(\frac{p}{2\pi}\right) \sin\alpha (a_1 \cos\theta - a_2 \cos\varphi) + \left(\frac{p}{2\pi}\right)^2 \cos\alpha, \tag{20}$$

and $y(\alpha, c)$ in the denominator is described as

$$\left\{ \begin{array}{c} (a_1\cos\theta - a_2\cos\varphi)^2 + \\ \left(a_1\sin\theta - a_2\sin\varphi\cos\alpha - \left(\frac{p}{2\pi}\right)^2 \varphi\sin\alpha - c\right)^2 + \\ \left[\left(\frac{p}{2\pi}\right)(\theta - \varphi\cos\alpha) + a_2\sin\varphi\sin\alpha - d\right]^2 \end{array} \right\}^{1/2}, \tag{21}$$

α represents the angle of the misalignment, and c is the lateral distance of the misalignment.

The disintegration of the equation components of the transmitting power and the power transfer efficiency for estimating the performances of the CCL-based WPT system topologies is provided in Figure 4a,b. The components constructing the transmitting power comprise the coupling coefficient, k, Q factor, and parasitic resistance. The coupling coefficient is proportional to the mutual inductance between the coupling coils and inversely proportional to the self-inductances. The mutual inductance can be derived using the Neumann formula with the radii, air gap, and number of turns of two coupling coils. The self-inductance can be derived by an inductance formula with a correction coefficient by feeding in the radius and number of turns of the coupling coil. Likewise, there are identical components in the expression of the power transfer efficiency.
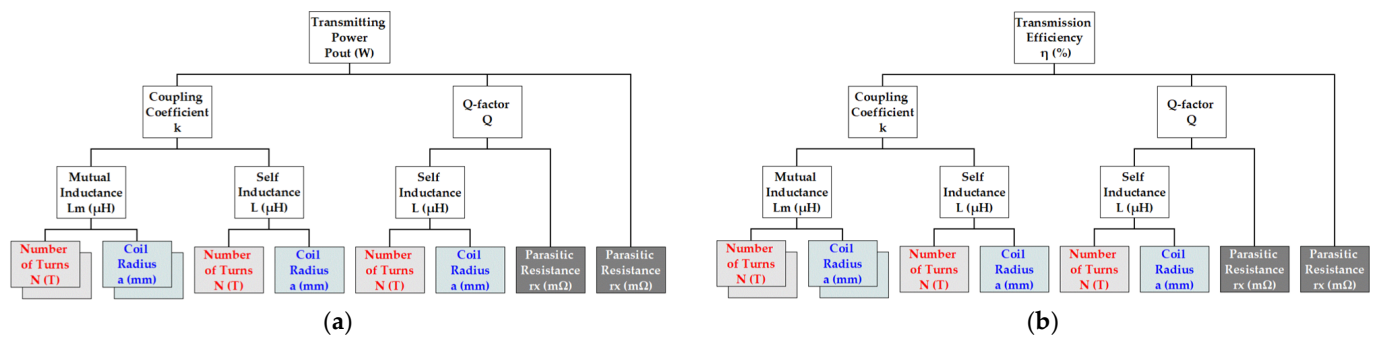

Figure 4. Separated diagrams of expressions for (**a**) transmitting power and (**b**) power transfer efficiency of the WPT system.

The coil radius, number of turns, and parasitic resistance are common parameters in these two estimated expressions for performance. These parameters were employed to observe the variations in the performances of the CCL-based WPT system topologies. The simulation process according to these coil parameters is illustrated in Figure 5.

Four steps were followed for simulating the transmitting power (1) and power transfer efficiencies (5) of the system topology. The first step involves the derivation of circuit elements. We derived the self-inductance and AC resistance of the coupling coil by relevant formulas and then combined the resistance and the reactance as the impedance for the coupling coil. We derived the DF by means of the equivalent circuit of the capacitor, given a capacitance to calculate the corresponding ESR. Likewise, we combined the ESR and the capacitance to find the impedance of the capacitor. Secondly, the circuits in the series or CCL topology were constructed from the derived impedances of the coupling coil and capacitors. We applied the drive voltage to the resonant circuit and produced the current flowing through the coupling coil. Afterward, the stored energy, power dissipation, and the Q factor can be derived further. Third, we employed the coil radius and the number

of turns of self-inductance to calculate the mutual inductance between two coupling coils. The coupling coefficient was also gained after the mutual inductance was divided by the self-inductance of the coupling coil. Finally, the transmitting power and the power transfer efficiency were derived from the coupling coefficient and the Q factor, and the performances of the CCL-based WPT system topologies were estimated. Moreover, the lateral distance and angle of misalignment were introduced in the performance estimation by following the four steps using the variables of coil geometry parameters. The air gap between the coupling coils was varied when the coupling coils were coaxially placed. Table 1 lists the parameters used in the simulations.
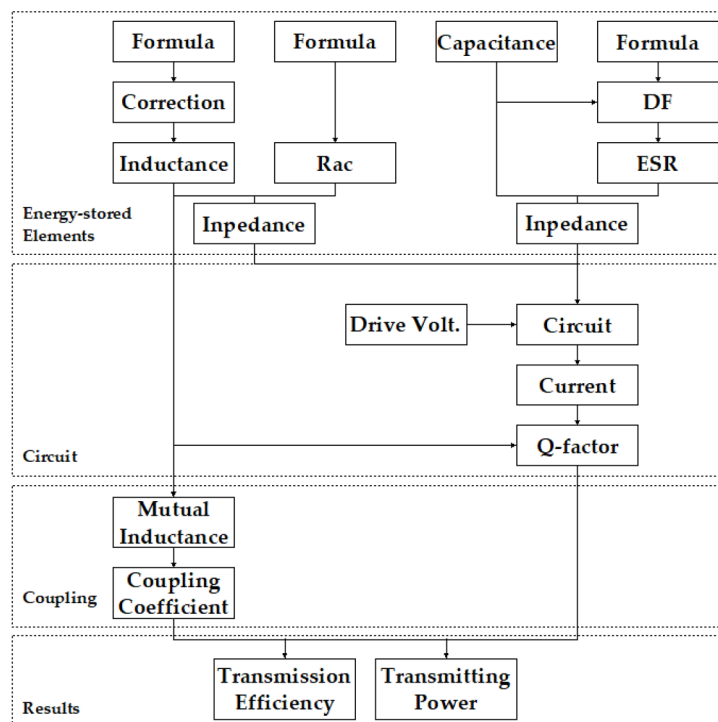
Figure 5. Process chart of the simulation for WPT system topology performance.

Table 1. List of parameters used in the simulations in this work.

Parameters	Symbol	Value
Radii of coupling coils on the transmitter	a_1	5–50 mm
Radii of coupling coils on the receiver	a_2	5–50 mm
Width of the conducting wire for the helical coil	D	1 mm
Air gap for coupling	g	2–6 mm
Lateral distance of misalignment	c	0–50 mm
Angle of misalignment	α	0–90°
Capacitance of the series capacitor in the CCL circuit	C_{XS} [1]	390 pF
Capacitance of the shunt capacitor in the CCL circuit	C_{XP} [1]	390 pF
Capacitance of the series capacitor in the series circuit	C_S	780 pF
Range of frequency sweep	f	2–2.14 MHz
Inner resistance of power source	r_S	1.2 Ω
Equivalent resistance of the system load	R_L	10 Ω
Drive voltage	V_S	24 V_{P-P}

[1] X in the subscript refers to the placement location, P is the transmitter, and S is the receiver.

As shown in Table 1, the width of conducting wire for the helical coil is 1 mm; the rated current for the wire is approximately 3 A according to the American wire gage. The rated voltage of the capacitors in the circuit is 100 Vdc in accordance with the general ceramic capacitor specification.

3. Results

The estimated result obtained in the study by Kim et al. (2021) [4] employing the varieties of the coupling air gap indicated that each topology has a different performance at the air gap, assuming that the operating frequency is fixed and parasitic resistance in elements is constant. The simulation for studying the performances of the CCL-based WPT system topologies was conducted following the process mentioned in the previous section. The air gap was fixed at 2 mm, and the coil radius and the number of turns were varied to observe the performance per topology within the frequency sweep range.

The self-inductance for the coupling coil and the parasitic resistance (Rac) were derived in advance. Likewise, the ESR was also derived by the relevant formula as Equation (8). The coil current was derived depending on the impedance of the coupling coil and the capacitors, and the circuit Q factor was calculated according to the coil current and the inductance. The simulation results of the Q factor are demonstrated in Figure 6a,b.
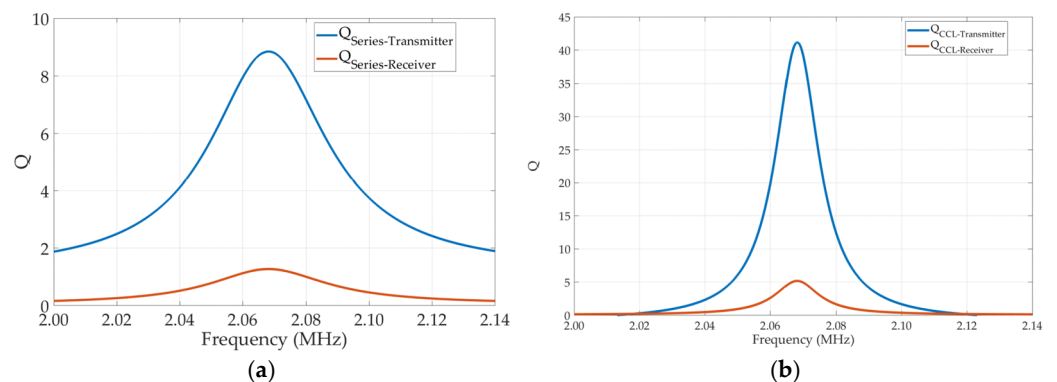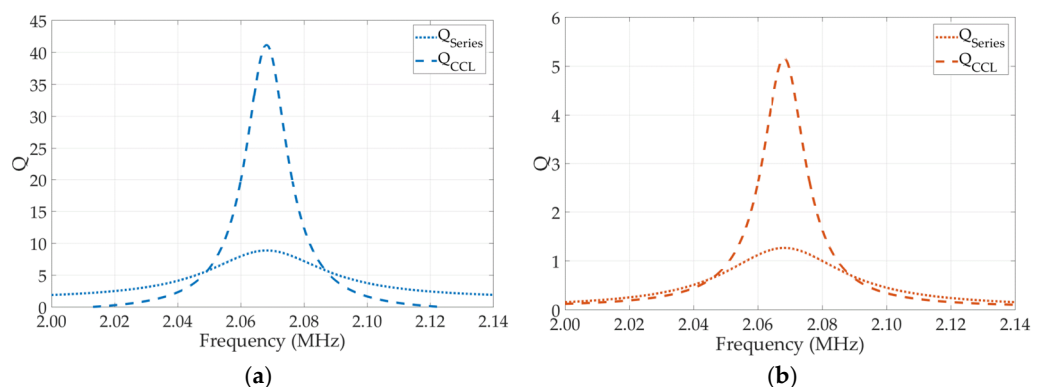

Figure 6. Q factor on the transmitter and receiver for (**a**) the series circuits and (**b**) CCL hybrid circuits.

Figure 6a shows the Q factor of the series resonant circuit within the frequency sweep range, including the Q factor curves when the series resonant circuit was applied to the transmitter and the receiver. Likewise, Figure 6b shows the curves of the Q factor for the CCL circuit, including those placed at the transmitter and the receiver.

The value of the Q factor is the maximum when the circuit operates at the resonant frequency. The maximum Q factor of the series resonant circuit placed at the transmitter is approximately 9, nine times that of the receiver. The maximum Q factor of the CCL resonant circuit at the transmitter is approximately 40, whereas it is 5 at the receiver.

Moreover, the Q factors of the series and CCL circuits were compared based on the location. Figure 7a shows the comparison of the Q factors on the transmitter, and Figure 7b shows that on the receiver. The Q factor of the CCL circuit is almost quadruple that of the series one, and identical circumstances exist for the receiver.

Figure 7. Comparison of Q factors between the series and CCL hybrid circuits when placed at (**a**) transmitter and (**b**) receiver sides.

Next, the Q factor in the topology was compared. The Q factor of the system topology is the product of the Q factors between the transmitter and the receiver. In this work, the system topologies simulated involved S–CCL, CCL–S, and CCL–CCL, and the S–S system topology was used for reference. The S–CCL system topology means that the transmitter uses the series resonant circuit, and the receiver uses the CCL circuit; the CCL–S system topology is the opposite of the S–CCL (the CCL resonant circuit is on the transmitter, and the series is on the receiver). In the CCL–CCL system topology, the transmitter and the receiver both use CCL circuits.

Figure 8 shows the Q factor curves of these system topologies. The CCL–CCL system topology has a substantial Q factor at the resonant frequency, whereas the Q factor of the S–S system topology is little. The Q factor of the CCL–CCL system topology is nearly quadruple those of the S–CCL and CCL–S system topologies and is greater than the S–S topology 10 more times.
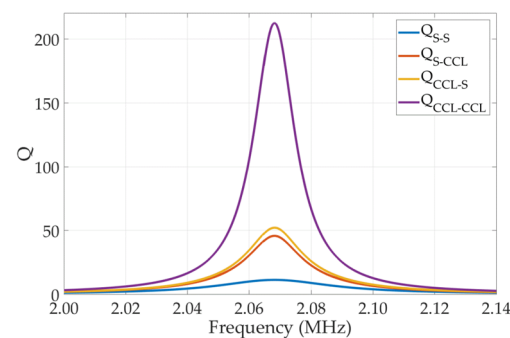
Figure 8. Comparison of Q factors among S–S, S–CCL, CCL–S, and CCL–CCL system topologies.

Subsequently, the coupling coefficient was derived based on the mutual and self-inductances of the coupling coil. The self-inductance of the helical coupling coil depended on the coil radius and the number of turns. The mutual inductance between two helical coupling coils was derived using the Neumann formula assuming no misalignment between two coupling coils.

The coil radius ranged from 5 to 50 mm, and the number of turns varied from 2 to 6 T. The alteration of the coupling coefficient, k, is shown in Figure 9.
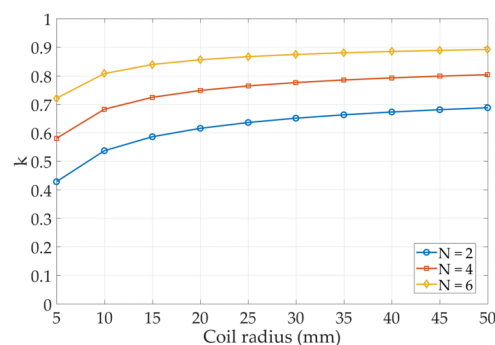
Figure 9. Coupling coefficient variation with coil radius and the number of turns.

Figure 9 shows that increasing the radius and number of turns of the helical coil can raise the coupling coefficient in the case of an identical air gap. The increased coil radius can increase the coupling coefficient for the same number of turns. Likewise, the increased number of turns can also increase the coupling coefficient for the same coil radius.

Noticeably, the coupling coefficient increased, implying that the mutual inductance also increased. The increment of mutual inductance led to the deviation in the resonant frequency. The variation of the resonant frequency is shown in Figure 10.
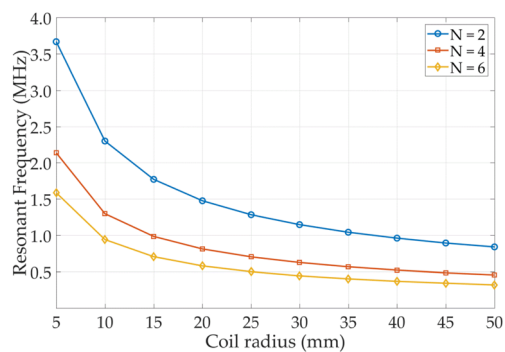
Figure 10. Resonant frequency variation with coil radius and the number of turns.

As shown in Figure 10, the increased coil radius leads to the deviation of the resonant frequency. Likewise, the deviation of the resonant frequency becomes moderated when the coil radius increases to a certain extent. The number of turns and coil radii have distinct resonant frequency deviations, e.g., for the helical coupling coil with six turns, the resonant frequency reaches 1.5 MHz when the coil radius is 5 mm; as the radius increases, the resonant frequency can fall under 0.5 MHz.

After obtaining the Q factor and the coupling coefficient, the transmitting power and the power transfer efficiency were calculated using the values obtained.

According to the parameters in Table 1, the performances of the topologies were estimated using four turns for the power-transmitting and power-receiving helical coils and a drive voltage of 24 V. The results are shown in Figure 11. Additionally, the resonant frequency for the simulated results is reduced to 600 kHz from 2.3 MHz with variations in the geometric parameters of the coupling coil.
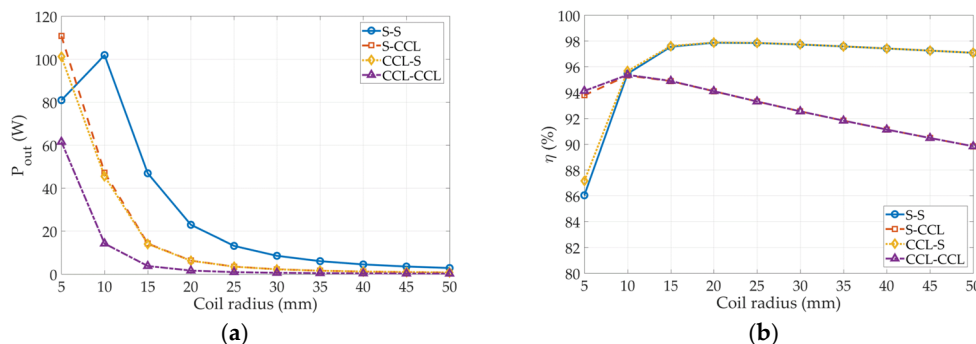

(a)

(b)

Figure 11. (a) Transmitting power and (b) power transfer efficiency variation with coil radius for WPT system topologies.

Figure 11a displays the transmitting power for the topologies versus the radii of the power-transmitting and power-receiving helical coils. Herein, the radius of the power-transmitting helical coil equals that of the power-receiving one. The tendencies of transmitting power for topologies fall with the increased radius. The S–S topology has the maximum transmitting power when the helical coils are 10 mm, which exceeds that when the radii are 5 mm; afterward, the transmitting power falls with the increased radii.

Figure 11b shows the power transfer efficiencies of the topologies versus the radii of the helical coil. Based on the variation of the power transfer efficiency with the radius of the helical coil, two distinct tendencies exist: the S–S and CCL–S topologies have a smaller efficiency when the radii are 5 mm, and the maximum efficiency is reached when the radii are 15 mm; afterward, it slightly decreases with the increase in the radii, whereas the S–CCL and CCL–CCL topologies have a greater power transfer efficiency when the radii are 5 mm, and the maximum efficiency appears at radii of 10 mm, after which the efficiency decreases significantly with the increased radii.

Figure 12 shows the transmitting power versus the coil radius and the number of turns for each topology corresponding to the resonant frequencies reduced from 2.3 MHz to 600 k Hz.
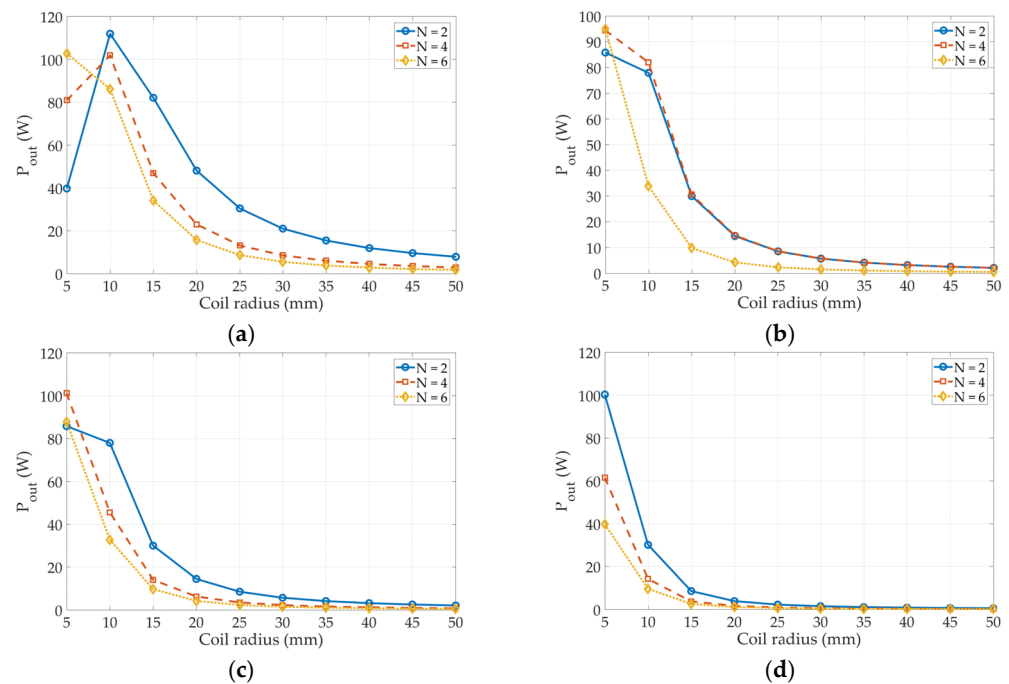
Figure 12. Comparison of output powers at various coil radii and numbers of turns for (**a**) S–S, (**b**) S–CCL, (**c**) CCL–S, and (**d**) CCL–CCL topologies.

As shown in Figure 12a, the transmitting power of the S–S topology decreases with the increase in the number of turns. There is an evident reduction in the transmitting power (approximately 10 W) when the radius of the helical coil is 10 mm. Interestingly, the maximum transmitting power appears at a helical coil radius of 5 mm when the number of turns increases to six turns; moreover, the maximum transmitting power appears at a helical coil radius of 5 mm, instead of 10 mm.

Figure 12b displays the transmitting power of the S–CCL topology; there is some reduction of the transmitting power when the number of turns decreases to two turns from four turns at a radius of 5 mm; there is only a slight reduction when the number of turns is 4 at a radius of 10 mm. Afterward, the transmitting power declined exponentially with the radius.
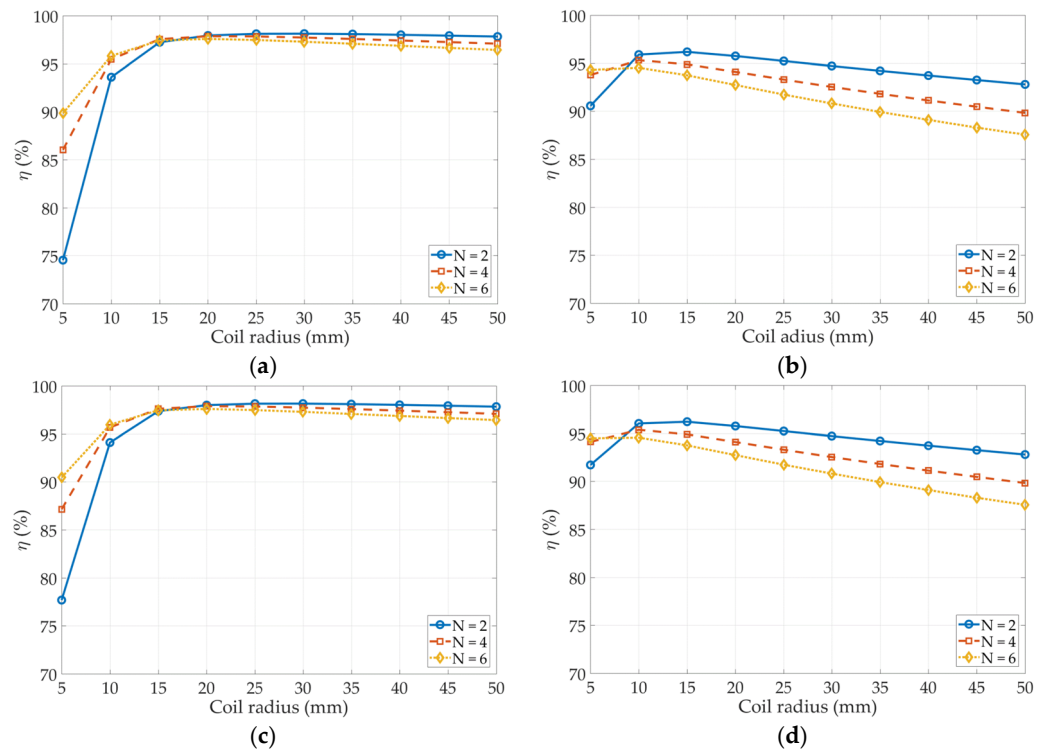
Figure 12c illustrates the transmitting power of the CCL–S topology in the variation of the number of turns and the radius of the helical coils. From Figure 12c, it is apparent that the maximum transmitting power can be obtained when the helical coil is set to four turns with a radius of 5 mm. Afterward, the transmitting power declined exponentially.

Figure 12d presents the variation of the transmitting power for the CCL–CCL topology with the number of turns and the radius. It is clear that the transmitting power decreases with the increased number of turns; similarly, it declines exponentially.

The efficiencies of these system topologies are also individually plotted based on the coil radius and the number of turns.

Figure 13 shows the transfer power efficiency for various topologies versus the number of turns and the radius during the resonant frequencies from 2.3 to 0.6 MHz. Noticeably, there are two tendencies in power transfer efficiency. Firstly, that has a sharp rise before the radius of 15 mm when the series circuit is used on the receiving side, namely S–S and CCL-S system topologies; afterward, the variant of power transfer efficiency becomes gentle with the radius increasing. Another one, the variance of power transfer efficiency is not severe

when the CCL circuit is placed on the receiving side; however, with the number of turns increasing, the power transfer efficiency will decline more.

Figure 13. Power transfer efficiencies at various coil radii and numbers of turns for (**a**) S–S, (**b**) S–CCL, (**c**) CCL–S, and (**d**) CCL–CCL topologies.

The transmitting power obviously decreased with the radius of the helical coil; it appears that the decrease in the transmitting power is due to the parasitic resistance on the circuits. In Equation (1), the product of the transmitter and receiver efficiencies suffers from the parasitic resistance because of the inner resistance of the power source, the equivalent resistance of the load, and the parasitic resistance in energy-storing elements. The inner resistance of the power source and the equivalent resistance of the load were assumed constant in this work. The efficiencies of the transmitter and the receiver in the transmitting power equation are affected by the parasitic resistances of energy-storing elements with the variation of the helical coil geometry.

Figure 14 presents the alteration in parasitic resistances with the helical coil geometry. As displayed in Figure 14a, the resistance increases reasonably with the radius.
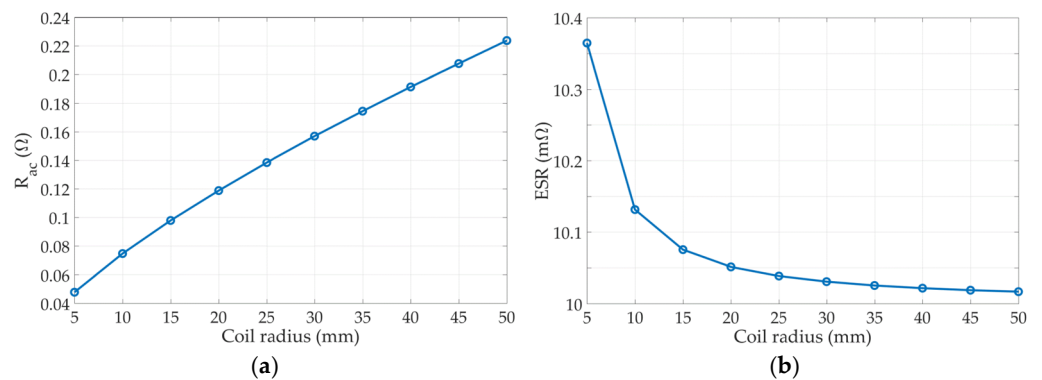
Figure 14. (**a**) Resistance in AC for the helical coil and (**b**) equivalent series resistance (ESR) for the capacitor.

The ESR of the capacitor is represented in Figure 14b. The ESR decreases with the radius of the helical coil, differing from the parasitic resistance of the helical coil. According to the definition of the ESR in Equation (8), it is related appreciably to the operating frequency. However, the variable in the ESR resistance is the radius of the helical coil, and the alteration in the radius shifts the resonant frequency. Therefore, the ESR of the capacitor varies with the radius of the helical coil.

The parasitic resistances of energy-storing elements are the components of the efficiencies for the transmitter and the receiver. It could be speculated that the magnitude of the efficiencies is affected by the radius of the helical coil. The alteration of the efficiencies for the transmitter and the receiver with the radius of the helical coil is plotted in Figure 15a,b, respectively. Apparently, the magnitude of the efficiencies, regardless of the transmitter or the receiver, reduces with the radius. The efficiency of the series circuit has less reduction, whereas the efficiency of the CCL circuit is remarkable. In summary, the simulated results showed that the transmitting power inevitably decreases with the radius of the helical coil due to the parasitic resistances.
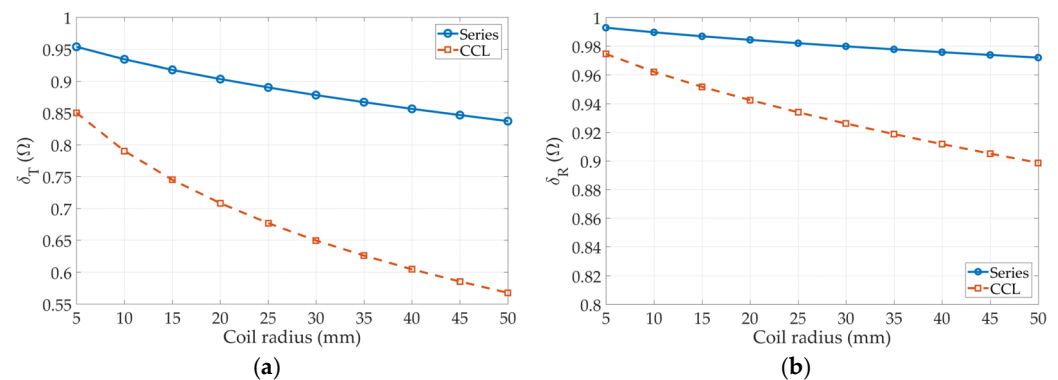

Figure 15. (**a**) Transmitter efficiency and (**b**) receiver efficiency.

The variation in the geometry of the helical coil changes the mutual inductance, shifting the resonant frequencies for the system topologies.

According to the Neumann formula shown in Equation (18), the air gap also affects the magnitude of the mutual inductance.

The effects of the varied air gap on the transmitting power and the power transfer efficiencies for the topologies are represented respectively in Figure 16a, b. The resonant frequencies of the system topologies reduce from 2.3 to 1.5 MHz; the variant magnitude in the resonant frequency is less than the variation of the geometric parameters of the coupling coil. The air gap range from 2 mm to 200 mm is shown; the geometry of the helical coil uses a radius of 50 mm and six turns. In the simulated results, the S–S topology has the maximum transmitting power at an air gap of 100 mm, then reduces gradually once the air gap increases continuously. For the S–CCL topology, the maximum transmitting power is obtained at an air gap close to 140 mm; for the CCL–S topology, it is at approximately 120 mm, and for the CCL–CCL topology, it is at 160 mm. The maximum transmitting power for the S–S topology is greater than those for other topologies, while the CCL–CCL topology is smaller than others, but the air gap for coupling is the longest.

Interestingly, the power transfer efficiencies showed two distinct trends, similar to those observed for the power transfer efficiencies with the variation in the radius of the helical coil. The S–S and CCL–S topologies give greater power transfer efficiencies before the air gap increases to 100 mm, whereas CCL–S and CCL–CCL topologies give greater power transfer efficiencies once the air gap increases continually after 100 mm.

According to the Neumann formula considering the misalignment as in Equation (21), the mutual inductance still suffers from the misalignment, shifting the resonant frequency of the system topologies.
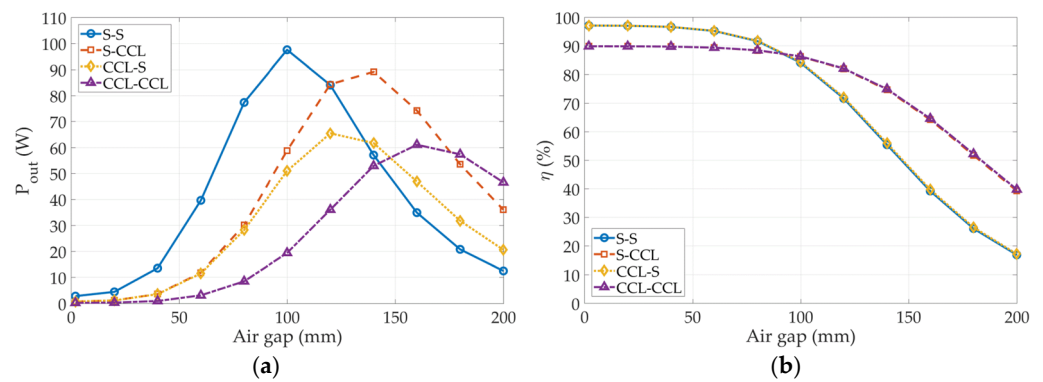
Figure 16. (**a**) Transmitting power and (**b**) power transfer efficiency of topologies at various air gaps.

The simulated results for the performance estimation of topologies are given in Figure 17. With the misalignment in lateral and angled, there is only a slight variation of the resonant frequency from 2.33 to 2.31 MHz. The simulated results were produced using the lateral misalignment distance in the range of 10–110 mm and the misalignment angle from 10 to 90 degrees. Figure 17a, b show the transmitting powers and power transfer efficiencies of the topologies in the case of lateral misalignment, and Figure 17c, d show those in angled misalignment.
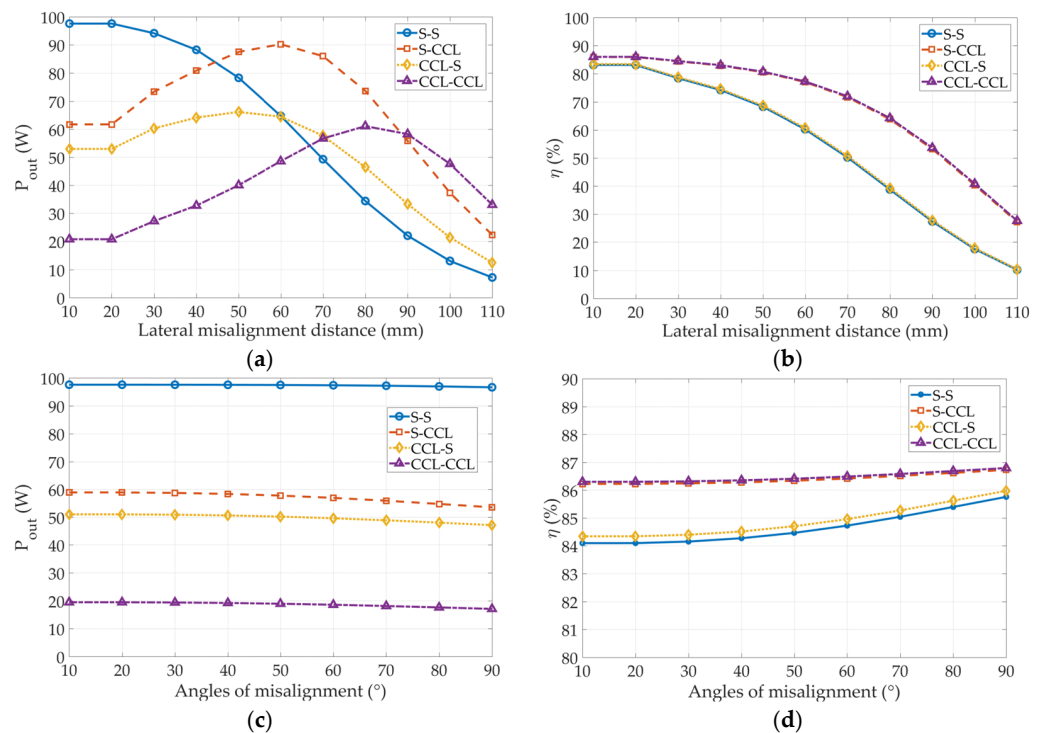

Figure 17. (**a**) Transmitting powers and (**b**) power transfer efficiencies for various topologies in lateral misalignment; (**c**) transmitting powers and (**d**) power transfer efficiencies for various topologies in angled misalignment.

With respect to the transmitting powers of topologies, there is a considerable variation with the lateral distance, whereas there is barely any variation for the transmitting power in angled misalignment.

The transmitting power of the S–S topology in lateral misalignment reduces gradually with the lateral distance. Notably, the topologies with the CCL circuit have no variation at lateral distances of 10 and 20 mm, but there is a variation when the lateral distance increases continually above 20 mm. While the transmitting power in the S–CCL topology

has the max. value at a lateral distance of 60 mm, the max. value of the CCL–S topology is obtained at 50 mm; the max. transmitting power of the CCL–CCL topology appears at 80 mm. Furthermore, the transmitting powers of the S–S and CCL–S topologies have similar values at 60 mm, which is approximately the same as that of the CCL–CCL topology at 70 mm. Regarding the transmitting powers of the topologies for angled misalignment, it appears that there is a negligible variation with the increased angle, only a difference in the magnitude of the transmitting power for various topologies. The S–S topology has the greatest, and the CCL–CCL has the smallest transmitting power.

Similarly, the variations in the power transfer efficiencies show two distinct trends. The power transfer efficiencies of topologies in lateral misalignment decline with the lateral distance; the S–S and CCL–S topologies show a significant reduction, while the S–CCL and CCL–CCL topologies show only a slight reduction in the power transfer efficiency. Conversely, the power transfer efficiencies of the topologies appear to rise with the increase in the angle of misalignment, regardless of the topology type. Nevertheless, the power transfer efficiencies of the S–S and CCL–S topologies significantly rise, whereas the variation is flat in the case of the S–CCL and CCL–CCL topologies.

4. Discussion

The prior study estimates the performance of the WPT system topologies using the CCL circuit at different air gaps, and estimation is conducted based on a fixed operating frequency, and the parasitic resistance in energy-storing elements has a constant value.

However, the resonant frequencies of the topologies vary with the air gap. In addition, the values of parasitic resistance will be different from the operating frequency, causing the power transfer of the topologies to be in a non-resonance state.

Likewise, this work estimated the performance of the WPT system topologies with the CCL circuit but simulated the performance by the relevant parameters of the helical coils using the corresponding resonant frequencies in various states. That can keep the system topologies in the resonance state to conduct optimal power transfer.

We found that the CCL circuit has a significant Q factor, whereas the Q factor of the series circuit is far less than that of the CCL circuit. When the CCL circuit is applied to the transmitter, the current flowing through the coupling coil is twice the power source when the series and shunt capacitances are identical. Nevertheless, the total parasitic resistance of the CCL circuit is greater than that of the series circuit, reducing the circuit efficiency and further attenuating the transmitting power of the topologies. Therefore, it can be seen from the simulated results that the transmitting power of the WPT system topologies with the CCL circuit is smaller than that of the S–S topology.

Interestingly, based on the variation of the power transfer efficiencies, two groups emerged. The first group involves the S–S and CCL–S topologies, and the second group involves the S–CCL and CCL–CCL topologies. When the CCL circuit is applied to the receiver side, their power transfer efficiencies decrease with the varied geometries of the helical coils. Contrarily, when the series circuit is applied to the receiver side, the power transfer efficiencies only slightly vary. Although the CCL circuit has a significant Q factor, it has a large parasitic resistance, which leads to circuit efficiency attenuation, reducing the transmitting powers of the topologies with the CCL on the receiver side with the varied geometries of the helical coils.

Subsequently, the performance of the system topologies is estimated with the variation in the distance of the coupling air gap. The transmitting powers of the system topologies show different trends; the coupling air gap acceptable for the S–S system topology is the shortest; relatively, the CCL–CCL system is the longest, whereas the coupling air gaps acceptable for the S–CCL and CCL–S topologies are identical. Nonetheless, the S–S system topology still has the maximum transmitting power, whereas the CCL–CCL topology has the minimum transmitting power. Although the acceptable coupling air gap for the S–CCL and CCL–S system topologies are identical, the magnitude of transmitting power differs. The discrepancy in the magnitude of the transmitting power could be

attributed to the circuit efficiency and circuit Q factors. Because the CCL circuit has a large parasitic resistance, attenuating the circuit efficiency. Hence, applying the CCL circuit to the receiver side shows a small circuit efficiency. Meanwhile, the circuit Q factor of the CCL circuit is far larger than that of the series circuit; thus, the product of the circuit Q factors for the transmitter and receiver sides differs. With regard to the maximum transmitting powers of the system topologies appearing at different air gaps, it could be interpreted that the magnitude of mutual inductance varies with the air gap, differentiating the coupling coefficient.

The power transfer efficiencies of the topologies decrease with the air gap. Likewise, the power transfer efficiencies are also divided into two groups. In the first group, the S–S and CCL–S system topologies have a higher power transfer efficiency at a shorter air gap until 100 mm; afterward, the power transfer efficiency renders a heavy decline. The other group has low efficiency within the air gap of 100 mm, but the amplitude of efficiency decline is small. When the CCL circuit is applied to the receiver side, its circuit efficiency is low, whereas it is high when the series circuit is applied to the receiver side.

For the effect of misalignment, the transmitting power shows drastic variations with lateral misalignment, while it is barely affected by angled misalignment. The power transfer efficiencies of the first-group topologies decrease in the case of lateral misalignment but increased in the case of angled misalignment. It could be because lateral misalignment reduces the magnitude of mutual inductance gradually with the lateral distance, whereas the increased misalignment angle slightly increases the mutual inductance.

By applying the CCL circuit to the receiver side, the system topology can provide a higher transmitting power to the load under the varied coupling air gap and lateral misalignment. Applying the CCL circuit to the transmitter and receiver sides transfers the power at longer distances of the air gap and lateral misalignment with the steady power transfer efficiency. Furthermore, the simulated results show that a low number of turns and a small radius of the coupling coil can contribute to the system topologies using CCL circuits to transfer the maximum power. In other words, a larger coupling coil has more parasitic resistance that can impact the performance of the system topologies.

These findings extend those of Kim and confirm the argument of Triviño that the parameters of the coupling coil have a direct effect on the performance of the WPT system.

In addition, this work reveals the properties of various system topologies under several circumstances and provides the relationship between the system topologies and the geometry of the helical coils. This work estimates the performances of the CCL-based WPT system topologies by providing an interactive relationship with the coupling coils, and the results can stimulate further developments in WPT technologies. The operating frequencies of the system topologies in this work employ corresponding resonant frequencies, which is challenging to realize in practice. Further work should focus on the capability of the frequency division in the controller and the power switching capability on the frequency, rendering the operating frequency closer to the practical resonant frequency.

The performance estimation for the WPT system topologies was simulated by employing theoretical derivation equations used in previous studies, which provide an understanding of the properties of WPT system topologies with CCL circuits. However, simulations may require the use of additional parameters for practical fabrication.

5. Conclusions

Our simulation results indicate that the performances of the CCL-based WPT system topologies decrease because of the coil parameters. Although there will be an appreciable effect of the Q factor on the CCL–CCL system topology, the transmitting power remains poor, which is attributed to the parasitic resistance of energy-storing elements. There are different representations of the transmitting power for the system topologies under various circumstances, except for the angular misalignment. Moreover, the transmitting powers for the system topologies with the CCL circuit show different trends with the air gap and misalignment. That could be interpreted as the variation of mutual inductance altering

the coupling coefficient. Simulating the performance of the system topologies in this work employs the corresponding resonant frequency to be the system operating frequency, ensuring that the system topologies are estimated in the resonance state. Appreciably, it is hard to achieve in practical design. The optimization of power transfer needs further clarification of the relationships among the coupling coil inductance, the compensation capacitance, and the system operating frequency.

Author Contributions: Conceptualization, C.-L.C.; methodology, C.-L.C.; resources, C.-W.H.; writing—original draft preparation, C.-L.C.; writing—review and editing, C.-W.H. All authors have read and agreed to the published version of the manuscript.

Institutional Review Board Statement: Not applicable.

Informed Consent Statement: Not applicable.

Data Availability Statement: Not applicable.

Conflicts of Interest: The authors declare no conflict of interest.

References

1. Kang, S.H.; Nguyen, V.T.; Jung, C.W. Analysis of MR-WPT using planar textile resonators for wearable applications. *IET Microw. Antennas Propag.* **2016**, *10*, 1541–1546. [CrossRef]
2. Kim, J.; Wei, G.; Kim, M.; Jong, J.; Zhu, C. A comprehensive study on composite resonant circuit-based wireless power transfer systems. *IEEE Trans. Ind. Electron.* **2018**, *65*, 4670–4680. [CrossRef]
3. Yang, K. Resonant Circuit Generates a High Frequency Magnetic Field Using this Resonant Technique. Available online: https://www.electronicdesign.com/technologies/analog/article/21806675/generate-a-highfrequency-magnetic-field-using-this-resonant-technique (accessed on 28 June 2018).
4. Kim, J.-G.; Kim, M.H.; Ko, M.-S.; Ro, K.C.; Jon, C.G. Study on CCL circuit-based WPT systems in consideration of parasitic resistances of circuit elements. *Electr. Eng.* **2021**, *103*, 2997–3004. [CrossRef]
5. Imura, T.; Okabe, H.; Hori, Y. Basic experimental study on helical antennas of wireless power transfer for Electric Vehicles by using magnetic resonant couplings. In Proceedings of the 2009 IEEE Vehicle Power and Propulsion Conference, Dearborn, MI, USA, 7–10 September 2009; pp. 936–940.
6. Imura, T.; Okabe, H.; Uchida, T.; Hori, Y. Study on open and short end helical antennas with capacitor in series of wireless power transfer using magnetic resonant couplings. In Proceedings of the 35th Annual Conference of IEEE Industrial Electronics, Porto, Portugal, 3–5 November 2009; pp. 3848–3853.
7. Triviño-Cabrera, A.; González-González, J.M.; Aguado, J.A. *Wireless Power Transfer for Electric Vehicles: Foundations and Design Approach*; Springer: Berlin, Germany, 2020.
8. Kim, J.; Wei, G.; Kim, M.; Ryo, H.; Ri, P.; Zhu, C. A splitting frequencies-based wireless power and information simultaneous transfer method. *IEEE Trans. Circuits Syst. I Regul. Pap.* **2018**, *65*, 4434–4445. [CrossRef]
9. Imura, T.B. *Wireless Power Transfer: Using Magnetic and Electric Resonance Coupling Techniques*; Springer Nature: Berlin/Heidelberg, Germany, 2020; pp. 48–49.
10. Lindquist, C. Capacitor DF and Q. *IEEE Trans. Comp. Hybrids Manufact. Technol.* **1978**, *1*, 115–117. [CrossRef]
11. Kim, J.; Wei, G.; Zhu, C.; Rim, C. Quality factor and topology analysis of the series-parallel combined resonant circuit-based wireless power transfer system. In Proceedings of the 2017 IEEE Transportation Electrification Conference and Expo, Asia-Pacific (ITEC Asia-Pacific), Harbin, China, 7–10 August 2017; pp. 1–5.
12. Bosshard, R.; Kolar, J.W.; Mühlethaler, J.; Stevanović, I.; Wunsch, B.; Canales, F. Modeling and η-α-Pareto optimization of inductive power transfer coils for electric vehicles. *IEEE J. Emerg. Sel. Top. Power Electron.* **2014**, *3*, 50–64. [CrossRef]
13. Van der Weijde, J.; Vlasblom, E.; Dobbe, P.; Vallery, H.; Fritschi, M. Force sensing for compliant actuators using coil spring inductance. In Proceedings of the 2015 IEEE/RSJ International Conference on Intelligent Robots and Systems (IROS), Hamburg, Germany, 28 September–2 October 2015; pp. 2692–2697.
14. Zhang, X.; Meng, H.; Wei, B.; Wang, S.; Yang, Q. Mutual inductance calculation for coils with misalignment in wireless power transfer. *J. Eng.* **2019**, *2019*, 1041–1044. [CrossRef]